Thermodynamic Comparison of Two Types of Stirling Refrigerators

Z.H. Wu[1,2], E.C. Luo[1], W. Dai[1], S.F. Li[1,2]

[1]Technical Institute of Physics and Chemistry
Chinese Academy of Science
Beijing 100080, China
[2]Graduate University of Chinese Academy of Sciences
Beijing 10049, China

ABSTRACT

The pulse-tube type of two-piston Stirling refrigerator can improve reliability by moving the expansion piston from the cold end to the ambient temperature end. More recently, the thermoacoustic-Stirling refrigerator further improves reliability by eliminating the expansion piston. The thermoacoustic-Stirling refrigerator uses a traveling-wave loop to achieve the Stirling cycle. Both refrigerators have a pulse tube. By means of thermodynamic analysis of the two refrigerators, this paper draws the following conclusions. Firstly, the pulse tube type of Stirling refrigerator can readily achieve any needed phase shifting by controlling the expansion piston, and it does not have to rely on the flowing resistance of the regenerator and the compliance and inertance effects of the different thermodynamic components that make contributions to phase shifting of the pressure and velocity waves. In contrast, the thermoacoustic-Stirling refrigerator is not able to perform active phase shifting, and its phase shifting mechanism is completely passive and somewhat dissipative because the flow resistance of the regenerator is a necessary part of the passive phase shifting. As a result, the pulse-tube type of two-piston Stirling refrigerator can achieve a little higher efficiency than the thermoacoustic-Stirling refrigerator. Secondly, the standing-wave acoustic field in the compression space of the thermoacoustic-Stirling refrigerator is predominant, resulting in smaller power flow for the same pressure wave amplitude and swept volume. In other words, the thermoacoustic-Stirling refrigerator may give smaller cooling power with the same working conditions and component sizes. Actually, the calculations show that the two-piston Stirling refrigerator gives a much larger cooling capacity than the thermoacoustic-Stirling refrigerator.

INTRODUCTION

Almost 170 years ago, the Stirling refrigerator was conceived for making ice. However, it was not until the 1950s that the first commercial Stirling refrigerator was developed by Philips.[1] According to the number of expansion and compression spaces, a Stirling system can be classified as either a single-acting Stirling system (with one expansion space and one compression space) or a double-acting Stirling system (with multiple cylinders). The single-acting Stirling refrigerator contains one compression piston and one expansion piston/displacer. The two-piston Stirling engine (see Fig.1 (a)) is always described as an ideal Stirling engine, which can achieve Carnot efficiency.

Cryocoolers 14, edited by S.D. Miller and R.G. Ross, Jr.

The expansion piston/displacer, which is used to recover expansion work, always performs phase control between the pressure oscillation and the velocity oscillation. Furthermore, the expansion piston/displacer suffers from a large temperature gradient between room temperature and low temperature, and it should have a poor thermal conductivity and long thermal conduction path to give good heat insulation for the cold-end. In general, the expansion piston/displacer in the Stirling refrigerator must work in the low temperature environment; this can bring serious problems with lubrication, sealing, friction etc.

Here we designed a pulse-tube type of Stirling refrigerator (PTSR) shown in Fig.1(b), in which the expansion piston is moved to the ambient surroundings by placing a pulse tube (PT) between the cold-end and hot-end heat exchangers (HX). The PT is originally used to replace the cryogenic displacers in the Stirling coolers[2], and it can greatly improve the reliability of the Stirling refrigerator. An ideal PT can act as a free gas piston when laminar flow is realized, and heat leakage to the cold end is only caused by the longitudinal heat conduction of the working gas. In the PTSR, any phase shifting can be achieved by controlling the phase difference between the compression and expansion pistons.

Recently, the invention of the work-recovery pulse tube refrigerator[3] was a milestone advance in developing a non-moving-part thermoacoustic refrigerator; this innovation can in principle improve the efficiency over the conventional pulse tube refrigerator. This new kind of pulse tube refrigerator is also called a thermoacoustic-Stirling refrigerator (TASR), and so far, great achievements have been made in its room-temperature cooling range.[4,5] Usually, the TASR has a loop configuration shown in Fig.1(c). Compared with the PTSR, the configuration of the TASR is made much simpler by utilizing an inertance tube and a compliance bulb instead of the mechanically moving expansion piston in the PT Stirling refrigerator. Actually, the inertance tube and compliance bulb are simply used to control the phase difference between the pressure wave and the volume flow rate wave in the regenerator.

Our objective here is to thermodynamically compare the PTSR and TASR via theoretical computations. In our numerical simulation, the phase shifting mechanisms of the expansion piston in the PTSR and the inertance tube and compliance bulb are investigated in detail. Optimization computations are performed to achieve the best performance of each refrigerator while keeping the same configurations of the regenerator, two ambient heat exchangers, the PT, the compression piston swept volume, and the same working parameters including frequency and mean pressure in both the PTSR and the TASR. After that, the distributions of temperature, the phase difference between pressure wave and volume flow rate wave, and several important power flows in the two refrigerators are given. In the first section of this paper, the PTSR and the TASR are introduced. In the second part, the numerical model in terms of linear thermoacoustic theory is briefly presented. Then, the thermodynamic analysis of the PTSR and TASR is carried out. Lastly, some conclusions are drawn.

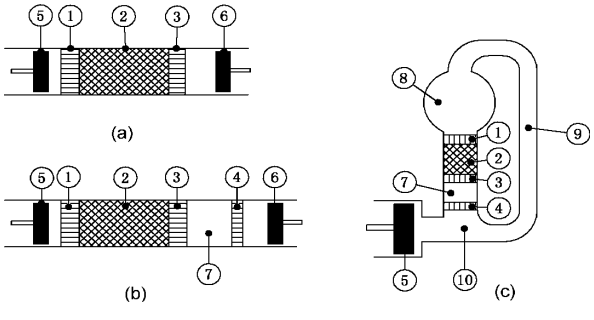

Figure 1. Schematic diagram of (a) the conventional two-piston Stirling refrigerator (b) the pulse-tube type of two-piston Stirling refrigerator and (c) the thermoacoustic-Stirling refrigerator: 1) main ambient HX; 2) regenerator; 3) cold-end HX; 4) secondary ambient HX; 5) compression piston; 6) expansion piston; 7) pulse tube; 8) compliance bulb; 9) inertance tube; 10) Tee.

NUMERICAL COMPUTATIONAL MODEL

The computational model used here is based on linear thermoacoustic theory.[5-7] For any flow channel with temperature gradient in the axial direction, the one-dimensional wave equation can be rewritten as

$$\frac{d\hat{p}}{dx} = -R_2 \cdot \hat{U} \tag{1}$$

$$\frac{d\hat{U}}{dx} = -R_1 \cdot \hat{p} + R_3 \cdot \hat{U} \tag{2}$$

And the total energy equation is

$$\frac{dH}{dx} = Q \tag{3}$$

$$H = c_1 + c_2 \cdot \frac{dT_x}{dx} \tag{4}$$

where $\hat{p}$, $\hat{U}$ are complex amplitude of pressure wave and volume flow rate, T_x is the time averaged temperature of the working gas, H is the total power, and Q is the heat exchange between the environment and the working gas. R_1, R_2, R_3, c_1, c_2 are functions of the flow channel, working frequency, average pressure, Reynold number, mean temperature, etc.

The models should be divided into N elements. For the two nodes of any element, we can obtain the transfer matrix according to Eq. (1) and Eq. (2)

$$\begin{bmatrix} \hat{p}_{(n+1)} \\ \hat{U}_{(n+1)} \end{bmatrix} = TM_{2\times 2} \cdot \begin{bmatrix} \hat{p}_{(n)} \\ \hat{U}_{(n)} \end{bmatrix} \tag{5}$$

where TM represents the 2-by-2 transfer matrix. Using energy conservation relation at n^{th} element, we obtain

$$B_1 T_{x(n-1)} + B_2 T_{x(n)} + B_3 T_{x(n+1)} = B_4 \tag{6}$$

where B_1-B_4 are coefficients. Combining all elements, the $\hat{p}$, $\hat{U}$ and T_x distributions can be solved by iteration.

COMPUTATIONAL RESULTS AND ANALYSIS

In our models, both the PTSR and the TASR have a regenerator, two ambient HXs, cold end HX, and PT. However, the two refrigerators have differences in their phase shifting mechanism. The PTSR can achieve an appropriate p and U phase angle especially in the regenerator by controlling the expansion piston, whereas the TASR uses the inertance tube and compliance bulb to control the phase distribution. The first phase shifting mechanism seems more active and convenient than the latter, but the latter is much simpler in configuration and has no moving mechanical parts. Additionally, the volume flow rate at the piston surface and the temperature of the HXs are known as the boundary conditions of the computation. In this part, we compare the operating characteristics of the two refrigerators including not only their phase shifting mechanism, but also their thermal performance including cooling power, acoustic power consumption, and efficiency.

Before the computations, the dimensions of the common parts should be described; these are shown in Table 1. All heat exchangers are plate-fin exchangers made of copper; the clearance between two fins is 0.5mm, and the heat exchanging area of the main ambient HX, cold-end HX, and secondary-ambient HX are 0.117 m^2, 0.117 m^2 and 0.033 m^2 respectively. The regenerator is made of 150 mesh stainless steal screens. The swept volume of the compression piston is 88 cm^3 (a compressor with such a swept volume has been tested in our lab), and the working frequency is fixed at 20 Hz. The regenerator and PT are thermally insulated from the 300 K ambient environment. Helium is used as the working gas with a mean pressure of 2.5 MPa.

Table 1. Dimensions of some parts unchanged in the computation

	Main ambient HX	Regenerator	Cold-end HX	Pulse tube	Secondary ambient HX
Inner diameter (mm)	50	50	50	50	50
Axial length (mm)	35	80	35	50	10

The optimization objective was to obtain maximal cooling power at –80ºC. The optimization of the PTSR is made by adjusting the phase angle between the compression piston and the expansion piston, while the TASR is optimized by changing the diameter and length of the inertance tube and the volume of the compliance. After the optimization, the compression piston lags the expansion piston by 90º for the PTSR, and the inertance tube is 650mm long and 10mm in diameter and the compliance volume 170 cm^3.

Temperature Distribution

Figure 2 gives the temperature distributions in the TASR and PTSR. In our computational model, both the computation origins are located at the outlet of the compression piston balance position. In Fig. 2(a), the first section from 0-650mm is the inertance tube, then comes the compliance bulb, main ambient HX, regenerator, cold-end HX, PT, and secondary ambient HX. In Fig. 2(b), the main ambient HX, regenerator, cold-end HX, PT, and secondary ambient HX are placed successively. The temperature of the cold-end HX is set as 193 K (-80ºC), and the Nusselt number of forced convection between the working gas and the cold-end HXs is 10.

p and U Phase Difference Distribution

Figure 3 gives the phase angle, by which pressure wave p leads volume flow rate wave U, as a function of x position. From Fig. 3(a), a phase jump occurs from the compression space to the Tee at x=0 because of the feedback flow at the Tee. Through the inertance tube and compliance bulb, the p-U phase difference varies from -50º to 10º. Then, it increases about 10º through the main ambient HX because the HX is a narrow channel with little flow resistance. This phase shifting mechanism can be clearly explained by the symbolic impedance diagram of the lumped parameter method and its phasor diagram[7] shown in Fig. 4.

The symbolic impedance diagram of the lumped parameter model in Fig.4 is similar to an electrical circuit diagram, and the inertance tube, compliance bulb, and the HX are analogous to inductance, capacitance, and resistance in the circuit, respectively. The terms L, C, and R indicate inertance, compliance and resistance. In the phasor diagram, the phase angle of the

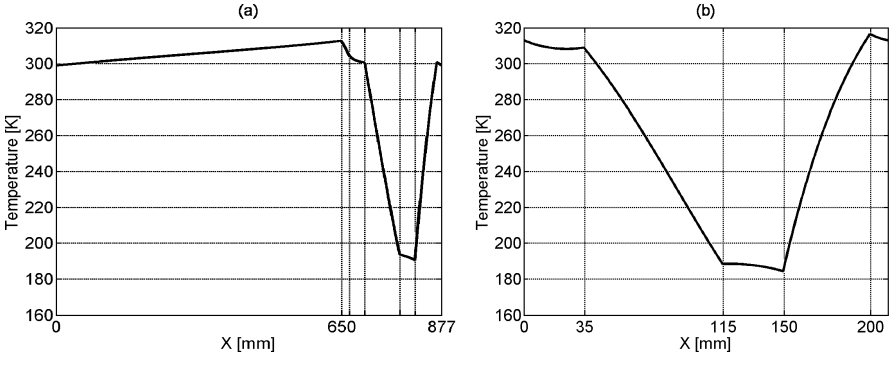

Figure 2. Temperature distributions of (a) TASR and (b) PTSR

volume flow rate U_1 leads the pressure phase angle p_1 by θ_1 at the beginning. Then the pressure drop dp_1 leads U_1 by 90º through the inertance, so p_2 lags U_1 by θ_2. In the compliance bulb, the volume flow rate drop dU_1 lags p_2 by 91º, so p_2 leads U_2 by θ_3. In the HX, dp_2 is out of phase with U_2 and p_3 leads U_2 by θ_4. This is the process of phase shifting created by the inertance tube and compliance bulb. Note that θ_1 to θ_4 strongly rely on the flow passage geometry.

Using the phase shifting mechanism, the regenerator can achieve a proper phase to reach a maximum cooling power. It is found that the TASR regenerator utilizes much of the standing-wave component of the acoustic field, and this will be a disadvantage for efficiency enhancement. Also, at the compression piston surface, p lags U by 81.5º at x=0, where the standing-wave acoustic field is predominant. However, at the middle of the PTSR regenerator, p and U are almost in phase, and the regenerator is mostly in the traveling wave acoustic field.

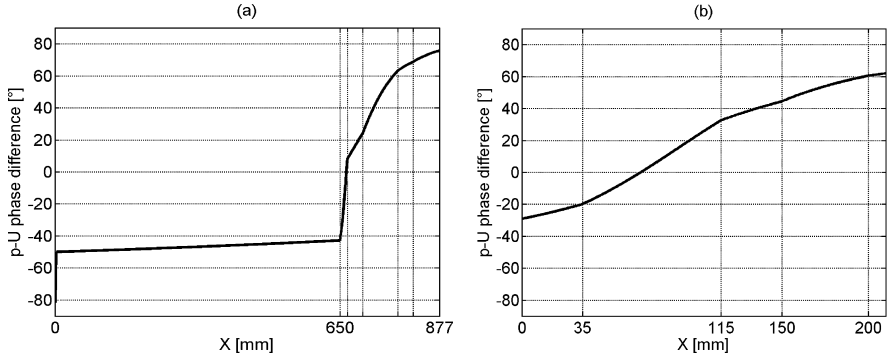

Figure 3. Distributions of phase difference between p and U of (a) TASR and (b) PTSR

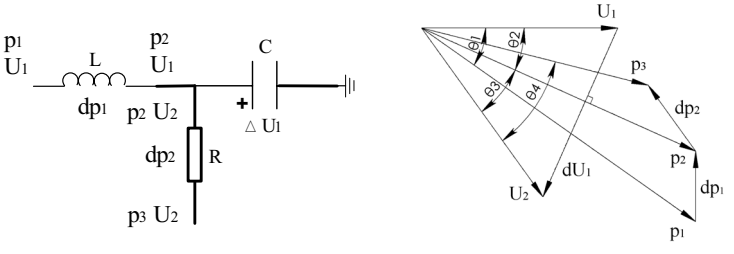

Figure 4. Diagram of symbolic impedance (left) and its phasor diagram (right) of TASR

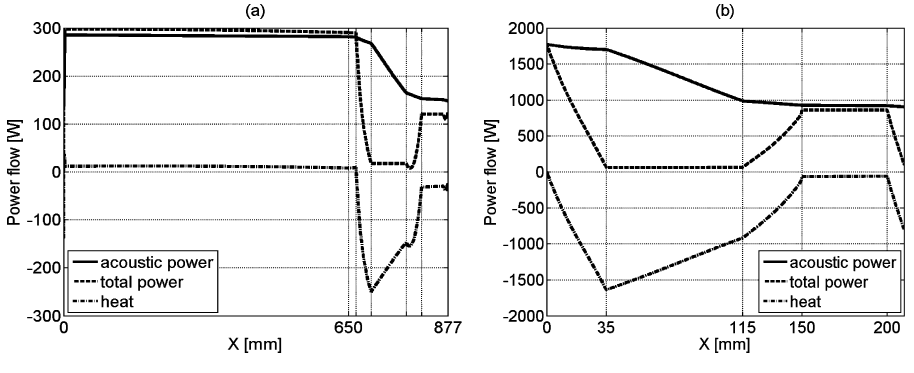

Figure 5. Power distributions of (a) TASR and (b) PTSR

Power Distributions

Power distributions are very important to understand in the refrigerator systems; they can be used to examine computational results and to calculate the cooling power, consumption power, etc. Figure 5 gives the power distributions of the TASR and PTST. Both in the TASR and the PTSR, the heat and the total power drop in the main ambient HX. This is because heat is carried away by cooling water, whereas acoustic power only decreases a bit; the total power is very close to 0 in the regenerator (because of thermal insulation from environment) but not equal to 0 (because of solid heat conduction). The cooling power is equivalent to the total energy difference between the outlet and inlet of the cold-end HX. In Fig. 5, the input powers of the two refrigerators are quite different — only 138 W before the 'Tee' in the TASR and about 865 W in the PTSR (calculated by subtracting expansion power from input power by compression piston). The reason for this is that: 1) the phase angle between p and U is close to 90^{o}, and 2) the void volume of the inertance tube and compliance bulb reduces the pressure oscillation amplitude when the total length is significantly smaller than 1/4 wavelength. The cooling powers are 103 W and 733 W for the TASR and PTSR, respectively. The COPs are 0.75 and 0.85, and the efficien-cies are 0.42 and 0.47.

CONCLUSIONS

After optimization of both refrigerators for maximum cooling power at -80° C, a numerical thermodynamic comparison of a TASR and a PTSR has been performed using a computational model based on linear thermoacoustic theory. For a reasonable comparison, the swept volume of the compressor piston, and the HXs, regenerator, and PT were assumed to be the same for the two refrigerators. However, the inertance tube and compliance bulb were changed for phase shifting in the TASR, and in the PTSR, the phase angle of the expansion piston was varied to achieve an appropriate phase distribution. The working gas was helium, charging pressure was 2.5 MPa, and frequency was 20 Hz. The phase shifting mechanism of the TASR is passive and complicated in principle because it depends on the dimensions of all of the components, frequency, and mean pressure, etc.— but the TASR is more reliable. In contrast, the phase shifting mechanism in the PTSR is active and easy to implement by simply controlling the expansion piston — but it has an additional mechanical part. According to our calculations, the standing-wave component is predominantly formed in the compression space of the TASR, resulting in little acoustic power input for the swept volume, whereas with the PTSR it is not. This important fact brings about a significant difference between the two systems in cooling power density. The consumed acoustic powers are 138 W for the TASR and 865 W for the PTSR. Furthermore, the PTSR is about 210 mm long and is much more compact than the TASR, which should be 877 mm long. The calculated maximum cooling powers are 103 W and 733 W for the TASR and PTSR, respectively, while the efficiencies are 0.42 and 0.47. The present study has not demonstrated that the PTSR has much higher efficiency than the TASR. In fact, the PTSR seems to have only a little better efficiency than the TASR.

ACKNOWLEDGMENT

This work was supported by the Natural Sciences Foundation of China (Grant No.50536040).

REFERENCES

1. Walker, G., *Cryocoolers Part 1: Fundamentals,* Plenum Press, New York (1983), pp. 95-104.
2. Radebaugh, R., Zimmerman, J., Smith, J., et al, "A comparison of three types of pulse tube refrigerator: new methods for reaching 60 K," *Adv.Cryog.Eng.*, vol.31 (1986), pp. 779-789.
3. Swift, G.W., Gardner, D.L., and Backhaus, S., "Acoustic recovery of lost power in pulse tube refrigerator," *J.Acoust. Soc. Am.*, vol. 105, no. 2 (1999), pp. 711-724.

4. Luo, E.C., Dai, W., Zhang, Y., et al, "Thermoacoustically driven refrigerator with double thermoacoustic-Stirling cycles," *Applied Physics Letters*, vol.88 (2006), pp. 074102.
5. Dai, W., Luo, E.C., Zhang, Y., et al., "Detailed study of a traveling wave thermoacoustic refrigerator driven by a traveling wave thermoacoustic engine," *J.Acoust.Soc.Am.*, vol.119, no.5 (2006), pp. 2686-2692.
6. Xiao, J.H. "Thermoacoustic heat transportation and energy transformation Part 1: Formulation of the problem," *Cryogenics*, vol. 35, no. 1 (1995), pp. 15-19.
7. Swift, G., *Thermoacoustics: A unifying perspective for some engines and refrigerators*, Fourth draft, 1999.